Paper No.
2462

A Thermodynamic Study of Hydrogen Sulfide Corrosion of Mild Steel

Jing Ning, Yougui Zheng, David Young, Bruce Brown and Srdjan Nesic
Institute for Corrosion and Multiphase Technology, Ohio University
342 West State Street
Athens, OH, 45701
USA

ABSTRACT

Expanding the basic knowledge required for improved understanding of hydrogen sulfide (H_2S) corrosion of mild steel is needed. When it comes to even the most basic chemical descriptors of aqueous H_2S systems such as: H_2S solubility, water chemistry, polymorphism of iron sulfide, the formation or dissolution of iron sulfide scale, and its protectiveness, many open questions persist and more investigation is required. Inconsistencies in prevailing expressions for H_2S solubility constant (K_{H2S}), the first dissociation constant ($K_{a,1}$) and the second dissociation constant ($K_{a,2}$) were reviewed here. By comparing with experimental data, the best prediction model for H_2S solubility and dissociation in an H_2S-H_2O system was identified. Occurrence of iron sulfide polymorphs was experimentally investigated and it was found that, in short term exposures, mackinawite formed at 25°C, while greigite and pyrite were detected at 60°C. The solubility limits for these iron sulfides were determined. Simplified Pourbaix diagrams for the H_2S-H_2O-Fe system have been constructed with different meta-stable and stable iron sulfides (mackinawite, pyrrhotite, greigite and pyrite) to predict the corrosion products in H_2S corrosion of mild steel.

Keywords: Hydrogen sulfide, polymorphous iron sulfide, Pourbaix diagram, solubility constant, dissociation constant, solubility limit

PART I THERMODYNAMIC STUDY OF A H_2S-H_2O SYSTEM

H_2S readily dissolves in water and partially dissociates. The reactions and the corresponding expressions with the solubility constants defining H_2S solubility and dissociation in an H_2S-H_2O system are shown as Equation (1) through Equation (6).[1] Solubility is directly related to the partial pressure of H_2S (pH_2S):

$$H_2S(g) \overset{K_{H2S}}{\Leftrightarrow} H_2S(aq) \tag{1}$$

$$K_{H_2S} = [H_2S]/p_{H_2S} \tag{2}$$

The partial dissociations occur in two steps; the first dissociation (Equation 3 and 4) is followed by the second dissociation (Equation 5 and 6):

$$H_2S \overset{K_{a,1}}{\Leftrightarrow} H^+ + HS^- \tag{3}$$

$$K_{a,1} = [H^+][HS^-]/[H_2S] \tag{4}$$

$$HS^- \overset{K_{a,2}}{\Leftrightarrow} H^+ + S^{2-} \tag{5}$$

$$K_{a,2} = [H^+][S^{2-}]/[HS^-] \tag{6}$$

Various expressions of the H_2S solubility constant (K_{H2S}), the first dissociation constant ($K_{a,1}$) and the second dissociation constant ($K_{a,2}$) are used for calculating the water chemistries in an H_2S-H_2O system.[1] Therefore, verification of these expressions is needed to determine the best expressions for calculation of water chemistries in the H_2S-H_2O system.

Experimental Setup

Due to inconsistencies of prevailing expressions for H_2S solubility and dissociation constants, experimental pH values were measured for verification purposes to check literature expressions and values for K_{H2S}, $K_{a,1}$ and $K_{a,2}$. The experimental apparatus used for this investigation is shown in Figure 1.

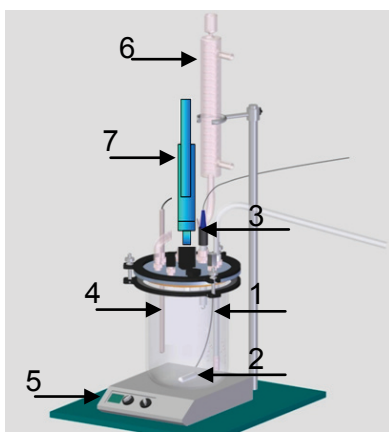

1. Sparge tube
2. Stir bar
3. pH probe
4. Temperature Probe
5. Heater
6. Condenser
7. Syringe

Figure 1. Experimental glass cell setup.

Experimental Procedure

The glass cell was filled with 2 liters of 1 wt.% NaCl solution. Experiments were conducted after purging this solution with N_2 until saturation (typically a few hours). The H_2S and N_2 pre-mixed gas was then purged into the solution at a desired partial pressure pH_2S. After the pH value stabilized, another pre-mixed gas with higher pH_2S was then purged into the solution, and the process was repeated. Experiments were performed for H_2S concentrations ranging from 40 ppm (pH_2S=0.0387 mbar at 25°C) to 8000 ppm (pH_2S=7.75mbar at 25°C) at 25°C, 60°C and 80°C. The relationship between pH_2S and measured pH value was obtained at 25°C, 60°C and 80°C.

Results and Discussion

Best known expressions for K_{H2S}, $K_{a,1}$ and $K_{a,2}$ were analyzed and combined into two models as shown in Table 1. The aim was to determine which of these models can best predict the pH, by comparing with experimentally determined pH values. Comparison of experimental pH with model predicted pH values at 25°C, 60°C and 80°C are shown in Figure 2, Figure 3 and Figure 4, respectively. The comparison shows clearly that Model 1 is superior to Model 2.

Table 1 Combinations of K_{H2S}, $K_{a,1}$ and $K_{a,2}$ in pH value prediction models

Models	K_{H2S}	$K_{a,1}$	$K_{a,2}$
Model1	Suleimenov,1994[2]	Suleimenov,1997[3]	Kharaka,1989[4]
Model2	Suleimenov,1994[2]	Kharaka,1989[4]	Kharaka,1989[4]

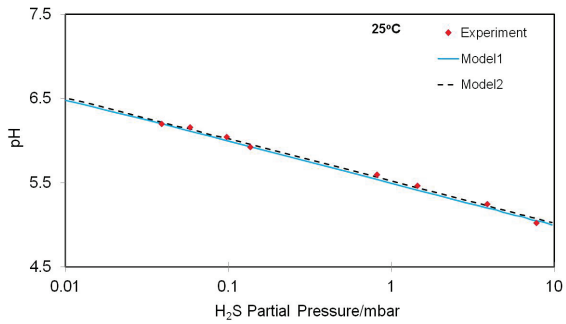

Figure 2. Comparison of experimental pH value with model predicted pH value at 25°C.

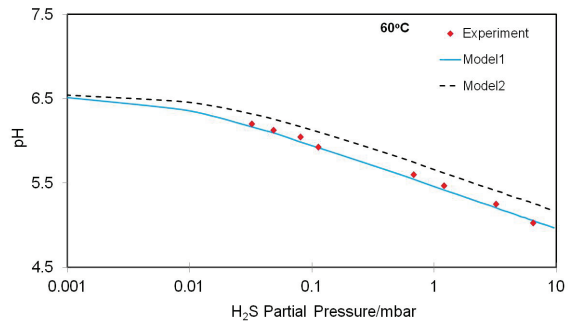

Figure 3. Comparison of experimental pH value with model predicted pH value at 60°C.

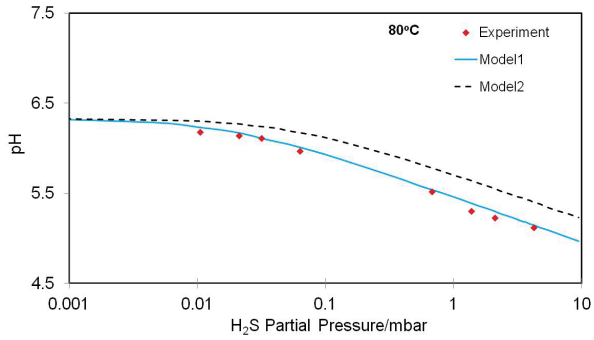

Figure 4. Comparison of experimental pH value with model predicted pH value at 80°C.

Summary

Comparison of experimental pH value with predicted pH value based primarily on the correlations provided by Suleimenov (1994 & 1997) showed an excellent agreement and therefore this model was selected to calculate water chemistry for a H_2S-H_2O system.

PART II THERMODYNAMIC STUDY OF A H_2S-H_2O-FE^{2+} SYSTEM

Polymorphs of iron sulfide are seen when it forms as a corrosion product in H_2S corrosion of mild steel, but the mechanisms related to the formation and transformation of various iron sulfides remain unclear. As a starting point, the solubility limits of various iron sulfides (K_{sp}) have been reviewed to gain better understanding of the formation and dissolution of a given iron sulfide layer, and how this may be related to its protectiveness. The current research initially focused on the solubility limit of mackinawite, as it initially forms as a corrosion product and, due to its meta-stability, can convert into other types of iron sulfide.[1] The solubility limit of mackinawite (K_{sp}) can be expressed at equilibrium conditions as shown in Equation (7) and (8) [1]:

$$\mathrm{FeS} + \mathrm{H}^+ \overset{K_{sp,2}}{\Leftrightarrow} \mathrm{Fe}^{2+} + \mathrm{HS}^- \tag{7}$$

$$\mathrm{K}_{\mathrm{sp},2} = \frac{[\mathrm{Fe}^{2+}][\mathrm{HS}^-]}{[\mathrm{H}^+]} \tag{8}$$

Many researchers have proposed solubility limit constants for mackinawite at 25°C; selected values for $K_{sp,2}$ from different literature sources are summarized in Table 2. Benning[5] proposed an equation relating $K_{sp,2}$ for mackinawite to temperature as shown in Equation (9):

$$K_{sp,2} = 10^{\frac{2848.779}{T_K} - 6.347 + \log(K_{a,1,H2S})} \tag{9}$$

Table 2. $pK_{sp,2}$ values for mackinawite from literature at 25°C.

$pK_{sp,2}$ of mackinawite at 25°C	Author
2.95	Berner,1967 [6]
3.55	Morse,1987 [7]
2.94	Theberge,1997 [8]
3.77	Benning,2000 [5]
3.5	Rickard,2006 [9]

A specific environment was defined here (25°C, pH_2S=0.97mbar, $[Fe^{2+}]$=10ppm, pH=6) and saturation value was calculated using Equation (10) with the various $pK_{sp,2}$ values for mackinawite as shown in Table 2. Calculated supersaturation (*SS*) values for the given conditions are shown in Figure 5.

$$SS = \frac{\dfrac{\left[Fe^{2+}\right]\left[HS^-\right]}{[H^+]}}{K_{sp,2}} \tag{10}$$

Note the variation of supersaturation values observed from Figure 5, due to differences in solubility product constants proposed by the various authors. According to Berner[6] and Theberge[8], the solution was close to saturation and the driving force for mackinawite precipitation was small. However, according to Benning[5], mackinawite supersaturation

was high and precipitation would readily occur. Supersaturation based upon $pK_{sp,2}$ values from Rickard[9] and Morse[7] lie somewhere in between. This indicates that further research is needed to confirm the $K_{sp,2}$ of mackinawite, as well as for other iron sulfides.

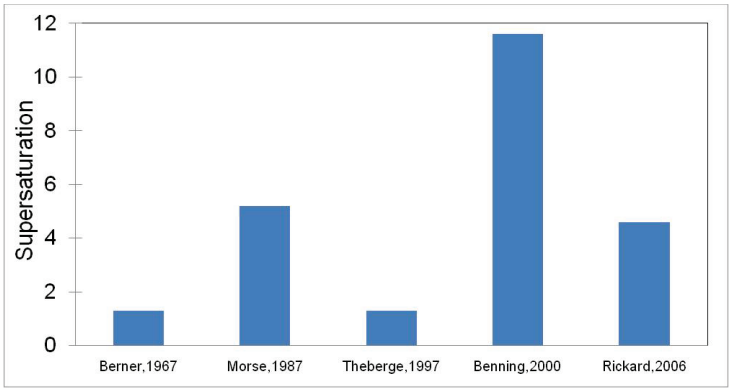

Figure 5. Calculated supersaturation using $pK_{sp,2}$ values in Table 2 for the selected environment (25°C, pH_2S =0.97mbar, $[Fe^{2+}]$=10ppm, pH=6).

Experimental Setup

The experimental apparatus used in this part of the study is shown in Figure 1. An syringe was used to add a deoxygenated ferrous chloride solution into the glass cell or to take sample solution from the glass cell.

Experimental Procedure

A method based on pH variation was used to judge reaction equilibria during precipitation and dissolution. From the iron sulfide reaction given by Equation (8), the pH value should be stable when this reaction reaches equilibrium. In experiments, this was considered to be the case when pH values varied by less than 0.01 units over a one hour time period. Dissolved iron concentration was measured spectrophotometrically and the hydrogen ion concentration was determined from the pH value at equilibrium. The bisulfide ion concentration was predicted from the previously verified H_2S-H_2O thermodynamic prediction model for hydrogen sulfide solubility and dissociation. The $K_{sp,2}$ value was calculated by Equation (8) at equilibrium.

In the experiments, nitrogen was purged into the 1 wt.% NaCl electrolyte until pH stabilized, then the H_2S / N_2 pre-mixed gas was introduced into the glass cell until saturation was achieved. Deoxygenated ferrous chloride solution was then injected into the glass cell. As no precipitation was typically observed, a deoxygenated 1.0 M sodium hydroxide was injected to increase pH and induce precipitation. The experiment was then left unperturbed and its pH value monitored. Then a deoxygenated 1.0 M hydrochloric acid was gradually injected into the glass cell to facilitate dissolution of an existing precipitate. This process was repeated to obtain other equilibrium points during precipitation and dissolution of various iron sulfides. Samples of the solution were taken from the glass cell and a 0.45 µm syringe filter was used to separate the precipitate from the solution before measuring ferrous ion concentration of the solution spectrophotometrically. The separation process was performed by filtration in an oxygen-free environment using a glove box. Recovered solid precipitate was dried in a nitrogen environment before XRD analysis.

Results and Discussion

Measured $pK_{sp,2}$ values of iron sulfide formed at 25°C

Three groups of experiments have been conducted to measure $pK_{sp,2}$ of formed iron sulfide: at 200 ppm H_2S with adding HCl to facilitate dissolution of precipitate, at 1000 ppm H_2S with adding HCl and at 200 ppm H_2S without adding HCl. The results for the 200ppm are shown in Figure 6. It was observed that measured $pK_{sp,2}$ values increased during the experiments starting at 2.87, then continued increasing to around 3.5. It was assumed that the $pK_{sp,2}$ value increased due to iron sulfide type changing. Precipitate filtered from the glass cell when $pK_{sp,2}$ was 3.48 was sent for X-ray diffraction to confirm this hypothesis.

Mackinawite, sulfur and lepidocrocite were detected by XRD, as shown in Figure 7. The precipitate ($pK_{sp,2}$ was 3.48) was totally black when it was filtered and dried, but the surface color turned yellow/brown when it was taken out to do analysis. Craig[10] and several others[11] also found the same: a mackinawite oxidation process, as given by Equation (11). Mackinawite is readily oxidized to form lepidocrocite and sulfur when it is exposed to an oxygen-containing environment.

$$FeS + 3O_2 + 2H_2O \rightarrow 4FeO(OH) + 4S \qquad (11)$$

The result for 1000 ppm H_2S also indictes that the $pK_{sp,2}$ value increased during the experiment, from 2.96 initially to 3.41. One more experiment for 200ppm H_2S without adding HCl to dissolve precipitate was performed to check whether the increased $pK_{sp,2}$ value was related to time of exposure or pH value. The same phenomenon was observed and $pK_{sp,2}$ increased during experiments even though no hydrochloric acid was added to adjust the pH. The data from these three experiments were combined and shown in Figure 8. Davison[12] reviewed current best estimates of $pK_{sp,2}$ at 25°C as shown in Table 3 and confirmed that amorphous iron sulfide formed during one to six hours of exposure time. The precipitate when $pK_{sp,2}$ was 3.48 at 200ppm H_2S was confirmed to be mackinawite by XRD. The three experiments shown in Figure 8 were consistent with Davison's review, suggesting that amorphous iron sulfide was formed initially ($pK_{sp,2}$ =2.95±0.1) then converted to mackinawite ($pK_{sp,2}$ =3.6±0.2).

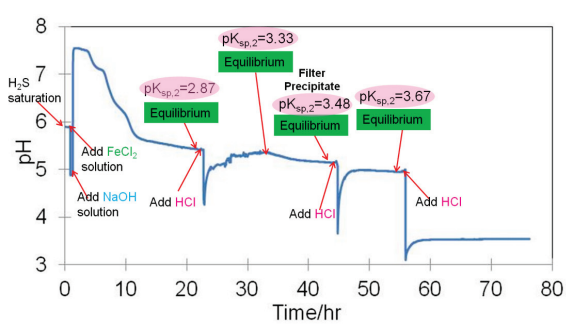

Figure 6. Measured $pK_{sp,2}$ at 200ppm H_2S with adding HCl at 25°C.

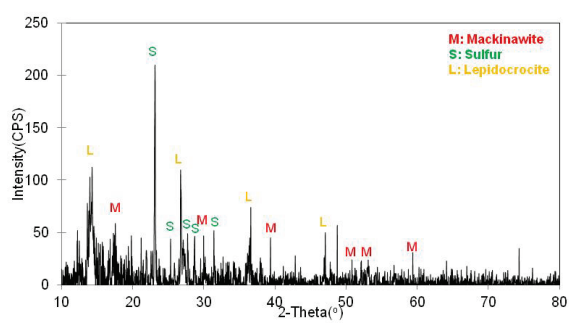

Figure 7. XRD of precipitate ($pK_{sp,2}$ was 3.48).

Table 3. Current best estimates of $pK_{sp,2}$ at 25°C from literature[12]

Amorphous FeS	2.95±0.1
Mackinawite	3.6±0.2
Greigite	4.4±0.1
Pyrrhotite	5.1±0.15
Troilite	5.25±0.2
Pyrite	16.4±1.2

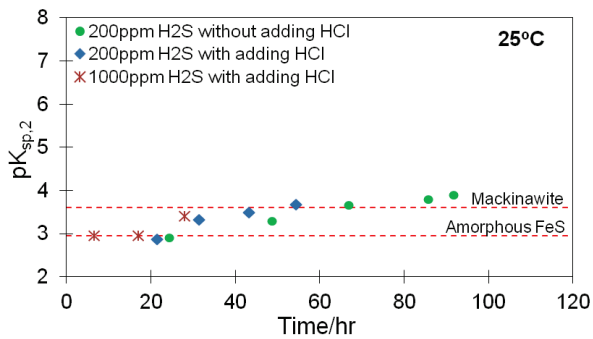

Figure 8. Summary of time dependence of $pK_{sp,2}$ at 25°C.

Measured $pK_{sp,2}$ values of iron sulfide formed at 60°C

Experiments were also conducted at 60°C with 200ppm H_2S and 1000ppm H_2S. The result of the 200ppm H_2S experiments is shown in Figure 9 and the repeated result is shown in Figure 10. It is easy to conclude that $pK_{sp,2}$ values can be divided into two groups: the "pH 3 group" and the "pH 6 group". It was assumed that the $pK_{sp,2}$ value difference was due to iron sulfide type changing, but whether this change was truly related to the pH value or an artifact of the experimental duration and sequence was unclear. Deoxygenated sodium hydroxide solution was added to adjust pH values from 3.3 to 5.0 and $pK_{sp,2}$ value decreased from 6.92 to 3.88 at the last point in Figure 10, which confirmed that $pK_{sp,2}$ value change was due to the pH value. Precipitate filtered from the glass cell when $pK_{sp,2}$ was measured to be 3.02 and 3.88 in Figure 10 was then sent for X-ray diffraction. Both greigite and pyrite were detected for these two samples, as shown in Figure 11 and Figure 12, with greigite being dominant.

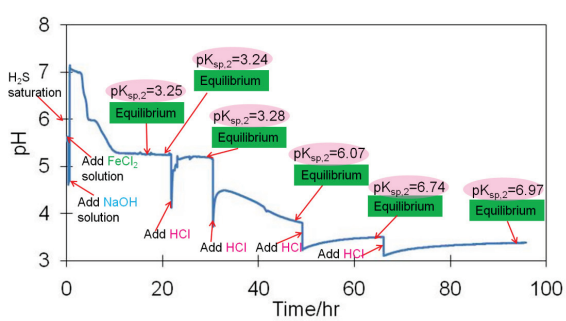

Figure 9. Measured $pK_{sp,2}$ at 200 ppm H_2S with adding HCl at 60°C.

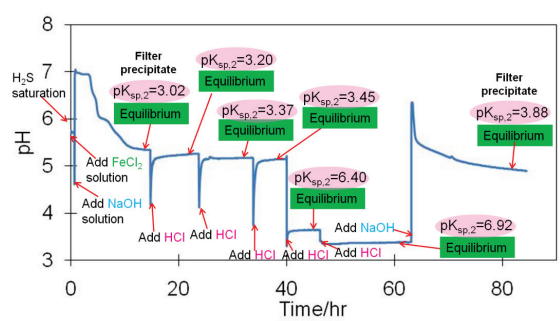

Figure 10. Measured $pK_{sp,2}$ at 200 ppm H_2S with adding HCl/NaOH at 60°C.

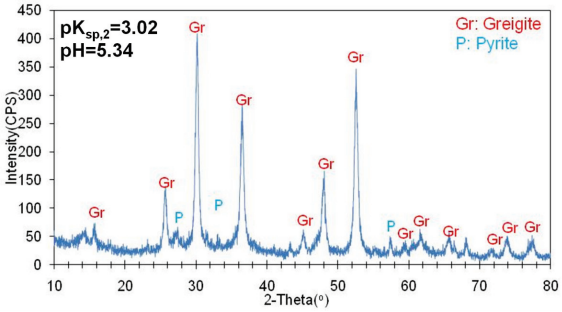

Figure 11. XRD of precipitate ($pK_{sp,2}$ was 3.02).

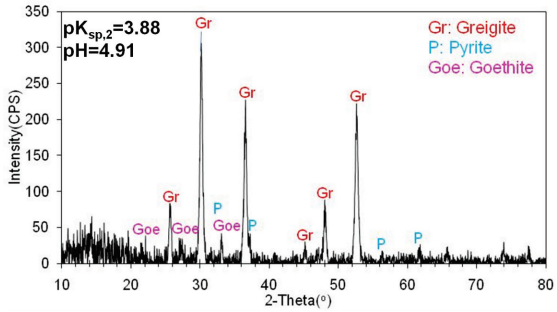

Figure 12. XRD of precipitate ($pK_{sp,2}$ was 3.88).

The results for 1000ppm H_2S are shown in Figure 13 and the repeated test is shown in Figure 14. It was also observed that the $pK_{sp,2}$ values differed between the "pH3 group" and the "pH6 group". The precipitate was filtered for analysis, taken when $pK_{sp,2}$ was 6.45 as shown in Figure 13 and taken when $pK_{sp,2}$ was 6.30 as shown in Figure 14. The XRDs of the precipitate is shown in Figure 15 and Figure 16, respectively. The XRD data with $pK_{sp,2}$ values of 6.45 and 6.30 showed that both precipitates were a mixture of greigite and pyrite with the latter being dominant. Therefore, it is postulated that pyrite is dominant for $pK_{sp,2}$ value "pH6 group" precipitates.

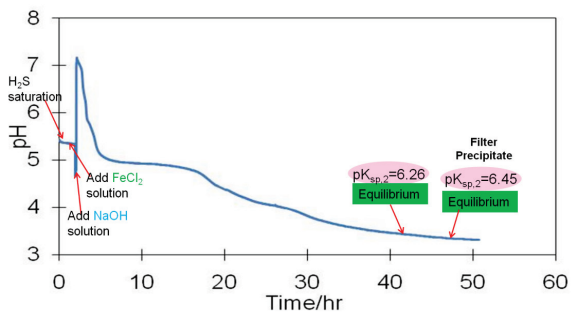

Figure 13. Measured $pK_{sp,2}$ at 1000 ppm H_2S without adding HCl at 60°C.

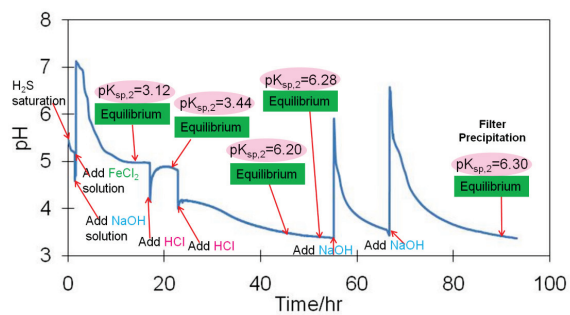

Figure 14. Measured $pK_{sp,2}$ at 1000 ppm H_2S with adding HCl/NaOH at 60°C.

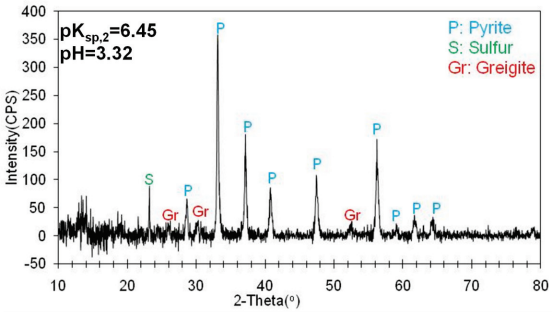

Figure 15. XRD of precipitate ($pK_{sp,2}$ was 6.45).

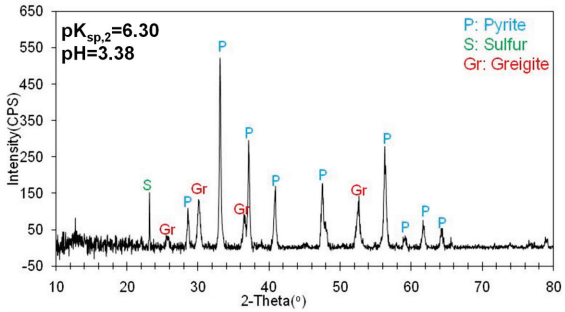

Figure 16. XRD of precipitate ($pK_{sp,2}$ was 6.30).

Recalculation of $pK_{sp,2}$ values of Greigite and Pyrite

Given their mineralogical importance, most research on iron sulfides has been conducted by geological scholars. Solubility reactions of greigite (Fe_3S_4) and pyrite (FeS_2) can be written as Equation (12) and Equation (14) according to Berner[6], Morse[7], Davison[12] and Rickard[13].

$$Fe_3S_4 + 3H^+ \overset{K_{sp,2}^{Greigite}}{\Leftrightarrow} 3Fe^{2+} + 3HS^- + S^0 \quad (12)$$

$$K_{sp,2}^{Greigite} = \left(\frac{[Fe^{2+}][HS^-]}{[H^+]}\right)^3 \quad (13)$$

$$FeS_2 + H^+ \overset{K_{sp,2}^{Pyrite}}{\Leftrightarrow} Fe^{2+} + HS^- + S^0 \quad (14)$$

$$K_{sp,2}^{Pyrite} = \frac{[Fe^{2+}][HS^-]}{[H^+]} \quad (15)$$

The $pK_{sp,2}$ values were recalculated as Equation (13) and Equation (15) shown for greigite and pyrite, respectively. The recalculation of $pK_{sp,2}$ values were plotted with pH value shown in Figure 17. Two groups can be seen from Figure 17, pyrite formed around pH 3.5 and greigite formed around pH 5.0.

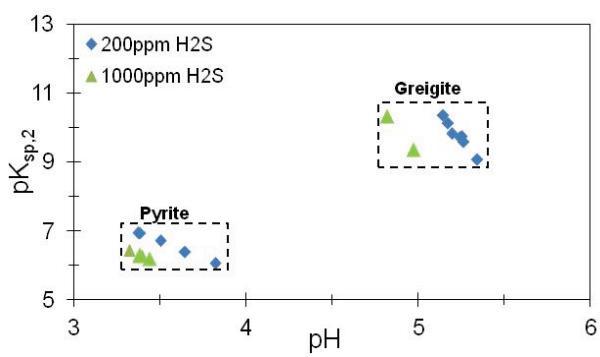

Figure 17. Summary of pH-recalculated $pK_{sp,2}$ at 60°C.

Summary

At 25°C, the measured K_{sp} values were observed to increase with time, due to iron sulfide type changing. It is believed that amorphous iron sulfide formed at the beginning then converted into mackinawite. Corresponding $pK_{sp,2}$ of mackinawite at 25°C was measured as 3.6 ± 0.2. Polymorphs of iron sulfides (pyrite and greigite) were observed in H_2S-H_2O-Fe^{2+} system at 60°C. For the investigated condition greigite was dominant around pH 5 with corresponding $pK_{sp,2}$ 9.8 ± 0.5, while pyrite was dominant around pH 3.5 with $pK_{sp,2}$ 6.5 ± 0.5.

PART III POURBAIX DIAGRAMS FOR A H_2S-H_2O-FE SYSTEM

Polymorphous iron sulfides can form in H_2S corrosion including amorphous iron sulfide (FeS), mackinawite (FeS), cubic ferrous sulfide (FeS), troilite (FeS), pyrrhotites ($Fe_{1-x}S$), smythite ($Fe_{3+x}S_4$), greigite (Fe_3S_4), pyrite (FeS_2) and marcasite (FeS_2).[14, 15] Some physicochemical properties of polymorphous iron sulfides are listed in Table 4.

Table 4 Polymorphous iron sulfides

Name	Chemical Formula	Crystal Structure	Properties
Amorphous	FeS	nano-crystalline	unstable, converts into mackinawite quickly
Mackinawite	FeS	Tetragonal, 2D layer	metastable, the initial corrosion product
Cubic FeS	FeS	cubic	very unstable, can transform into mackinawite, troilite or pyrrhotite, never found naturally
Troilite	FeS	hexagonal	stoichiometric end member of the $Fe_{1-x}S$ group(x=0)
Pyrrhotite	$Fe_{1-x}S$ (x=0 to 0.17)	monoclinic Fe_7S_8 or hexagonal $Fe_{10}S_{11}$	thermodynamically stable, the most abundant iron sulfide in the Earth
Smythite	$Fe_{3+x}S_4$ (x=0 to 0.3)	trigonal-hexagonal	metastable, related to the $Fe_{1-x}S$ group
Greigite	Fe_3S_4	cubic	metastable $Fe^{2+}Fe^{3+}$ sulfide
Pyrite	FeS_2	cubic	thermodynamically stable iron disulfide, the most abundant mineral on the Earth's surface
Marcasite	FeS_2	orthorhombic	metastable, common mineral in hydrothermal system and sedimentary rocks

Mackinawite, cubic ferrous sulfide, troilite, pyrrhotite, greigite and pyrite have all been detected as corrosion products for mild steel in previously reported small and large scale laboratory tests.[16-20] It is broadly believed that different corrosion products have different effects on mild steel corrosion in H_2S environments due to their different physico-chemical properties.[21, 22] Development and verification of a thermodynamic prediction model for corrosion products seen in H_2S corrosion of mild steel, is critical in an effort to better understand their effect on corrosion. This will also be of key importance for the development of corrosion mitigation strategies in sour systems.

Amorphous Iron Sulfide (FeS)

Amorphous iron sulfide can only be detected by X-ray diffraction as broadened low-intensity peaks, so usually it is assumed that it lacks any sort of long-range order (crystallinity). Kornicker[23] found that the physical properties of amorphous iron sulfide changed after drying, which might indicate that amorphous iron sulfide is a hydrate. Wolthers[24] used low angle X-ray powder diffraction (LAXRPD) to determine that "amorphous iron sulfide" is nanocrystalline mackinawite with an average particle size of 2.2 ± 1.7nm. Rickard and co-workers[25, 26] concluded that "amorphous FeS" does not exist. They also stated that "amorphous iron sulfide" which first precipitates from bulk solution is nanocrystalline mackinawite and confirmed that it is not hydrated by using nuclear magnetic resonance (NMR) spectroscopy and thermogravimetric analysis (TGA).

Mackinawite (FeS)

Mackinawite is widely considered to be the initial corrosion product in H_2S corrosion due to its rapid formation kinetics, and then converts into other iron sulfides depending on environmental conditions. The crystal structure of mackinawite consists of 2D layers, as shown in Figure 18 (a). The composition of mackinawite is usually stated as iron rich, $Fe_{1+x}S$ (x=0 to 0.11). Berner[6] reported $Fe_{0.91}S$, Sweeney[27] found $Fe_{1.09-1.15}S$, Ward[28] reported $Fe_{0.995-1.023}S$, and Lennie and Vaughan[29] proposed $Fe_{0.99\pm0.02}S$. It is Rickard[13]

who suggested that the reasons for previous researchers obtaining the composition of mackinawite as iron rich, $Fe_{1+x}S$, are due to an analytical artifact relating to the presence of other metals in mineralogical samples. Rickard[30] measured the composition of mackinawite as stoichiometric FeS.

Cubic Iron Sulfide (FeS)

The crystal structure of cubic iron sulfide is shown in Figure 18 (b). De Medicis[31] determined that cubic FeS did not form in the presence of oxygen or chlorides. Murowchik[32] also found that it can only crystallize at temperatures < 92°C and pH 2-6 in 4 to 85 hours, with its formation impeded by the presence of chlorides. Smith[21] concluded that cubic iron sulfide is a transitional product that degrades into mackinawite, troilite or pyrrhotite over several days and that it is not a major constituent of any long term corrosion product; it has only been observed in the laboratory, so it is not expected to be found in field conditions.

Cubic FeS has been detected in the so called top-of-the-line corrosion (TLC)[19], where pure condensed water is seen. It can be excluded from the current study which primarily focuses on the so called bottom-of-the-line corrosion, where chlorides are normally present in the produced water.

Pyrrhotite ($Fe_{1-x}S$ (x=0 to 0.17)) and Troilite (FeS)

Pyrrhotite is actually a non-stoichiometric group of iron sulfides with formulae corresponding to $Fe_{1-x}S$ (x=0 to 0.17), where troilite is the stoichiometric end member of the pyrrhotite group when x=0 (FeS). The crystal structures of pyrrhotite and troilite are shown in Figure 18 (c) and (d). Pyrrhotite and troilite are thermodynamically stable; these two co-exist below 150°C[33]. Troilite and pyrrhotite are differentiated only because the crystals that nucleate seem to initially grow differently at temperatures below 150°C. Troilite can be viewed as low temperature and stoichiometric pyrrhotite. A variety of different pyrrhotites have been observed with different values of x resulting in changes in the unit cells of each.

Smythite ($Fe_{3+x}S_4$(x=0 to 0.3))

Smythite is the least studied iron sulfide and has not been reported as a corrosion product,[21] so it can be excluded from most corrosion studies.

Greigite (Fe_3S_4)

The crystal structure of greigite is shown in Figure 18 (e). Greigite is thermodynamically metastable; Lennie[29] noted that greigite is often present as an intermediary between the initial corrosion product - mackinawite and the final product - pyrite.

Pyrite (FeS_2)

Pyrite is the most abundant sulfide mineral in nature, also known as "fool's gold". The lattice crystal structure of pyrite is shown in Figure 18 (f). Pyrite and pyrrhotite are the most stable iron sulfides, and considered to be the corrosion products seen in long exposures.

Marcasite (FeS_2)

Marcasite is compositionally identical to pyrite, but structurally different. Benning[5] found the absence of marcasite under both reducing and oxidizing conditions in corrosion testing. Marcasite is not a typical corrosion product and the publications related to marcasite are primarily in the geological literature such as the work of Schoonen[34] and Murowchick[32]. There is no clear evidence that marcasite appears in corrosion environments, so marcasite is not taken into consideration here to be relevant in corrosion studies.

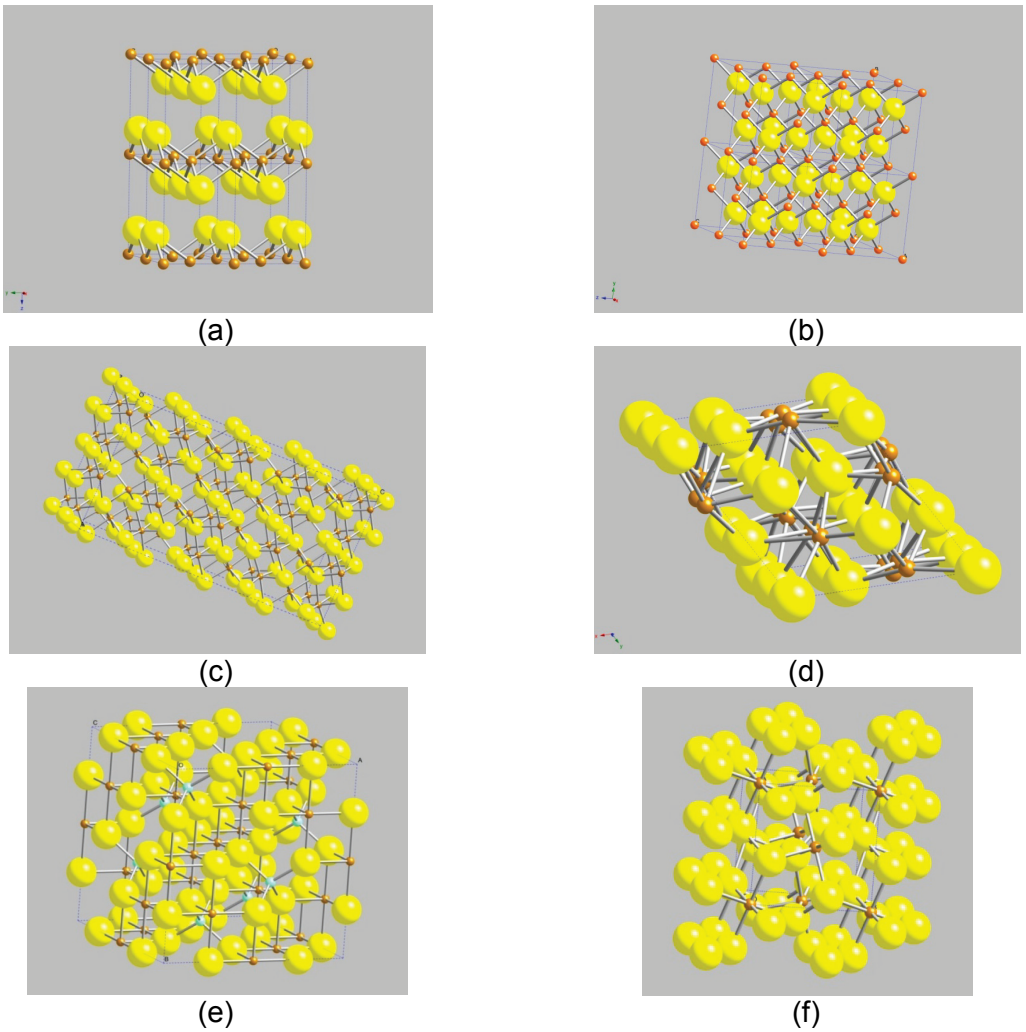

Figure 18. Crystal structures of: (a). mackinawite; (b). cubic iron sulfide; (c). pyrrhotite; (d). troilite; (e). greigite; (f). pyrite generated by CrystalMaker™.

Summary

The polymorphous character of iron sulfides have been classified above primarily based on whether they were found in corrosion of mild steel in oil and gas systems. This was done in order to generate relatively simple Pourbaix diagrams dedicated to internal pipeline corrosion environments. In summary: the iron sulfides that have been taken into consideration for generating Pourbaix diagrams below are: mackinawite, pyrrhotite, greigite and pyrite.

Construction of Pourbaix diagram for a H_2S-H_2O-Fe System at 25°C

A thermodynamic stability diagram (E vs. pH), also known as a Pourbaix diagram, is one of the most prominent contributions to corrosion science made by M. Pourbaix[35, 36]. Pourbaix diagrams are used to map behavior of metal in aqueous solution and thermodynamically stable corrosion products for practical purposes. Bouet[37] has developed Pourbaix diagrams for H_2S-H_2O-Fe system with iron sulfides FeS, FeS_2 and Fe_2S_3. Ueda[38] has generated Pourbaix diagrams for H_2O-CO_2/H_2S-Fe system with FeS and FeS_2. Anderko[39, 40] referred to a commercial software package used to calculate and plot Pourbaix diagrams including amorphous iron sulfide, mackinawite, greigite, marcasite, pyrite and stoichiometric pyrrhotite. Discrepancies between Pourbaix diagrams representing the same species associated with sour corrosion from these authors are due to variations in the sources of thermodynamic data, the different types of iron sulfides considered and the diversity of reactions considered. Moreover, the unknown background details pertaining to commercial software packages used for generation of Pourbaix diagrams makes it hard for corrosion engineers to understand and interpret the results they produce. Therefore, considering the relatively narrow corrosion focus in this study, development of Pourbaix diagrams for corrosion of mild steel in aqueous H_2S solutions is shown below in a stepwise fashion, accompanied by a complete account for all the assumptions, underlying thermodynamic data and reaction mechanisms.

As a starting point, Pourbaix diagrams for H_2S-H_2O-Fe system were constructed at reference temperature (25°C) and constant H_2S partial pressure.

Thermodynamic Background

Corrosion is an electrochemical process that includes reduction and oxidation reactions. From the first and second law of thermodynamics one can write:

$$\Delta G + zFE = \Delta \widetilde{G} \tag{16}$$

where, ΔG is free energy change of a chemical reaction, zFE is the electrical energy and $\Delta \widetilde{G}$ is the total free energy change of an electrochemical reaction. At electrochemical equilibrium, $\Delta \widetilde{G} = 0$, and Equation (16) becomes,

$$\Delta G = -zFE_{rev} \tag{17}$$

where, E_{rev} is the reversible potential at equilibrium.

After transformation, the Nernst equation is obtained to calculate E_{rev} of an electrochemical reaction at equilibrium for any given set of conditions,

$$E_{rev} = E^{o}_{rev} - \frac{RT}{zF}\sum_{i=1}^{\kappa} \ln(c_i)^{n_i} \tag{18}$$

where, E^{o}_{rev} is standard reversible potential which is defined at unit concentrations, reference temperature and reference pressure. It can be computed from,

$$E_{rev}^{o} = -\Delta G_r^{\ o} / zF \tag{19}$$

where, $\Delta G_r^{\ o}$ is the Gibbs free energy change of the electrochemical reaction.

For example, the iron deposition/dissolution reaction is an electrochemical reaction shown by Equation (20). The Gibbs free energy change of reaction (20) is expressed in Equation (21).

$$Fe^{2+} + 2e^{-} \Leftrightarrow Fe \tag{20}$$

$$\Delta G_r^{\ o} = G_{Fe}^{0} - G_{Fe^{2+}}^{0} - 2G_{e^-}^{0} \tag{21}$$

The standard reversible potential of reaction (20), $E_{rev(Fe^{2+}/Fe)}^{o}$, is calculated by Equation (19), and then it is substituted into Equation (18) to calculate reversible potential of the reaction (20), $E_{rev(Fe^{2+}/Fe)}$.

$$E_{rev(Fe^{2+}/Fe)} = E_{rev(Fe^{2+}/Fe)}^{o} + \frac{RT}{2F}\ln(c_{Fe^{2+}}) \tag{22}$$

For a pure chemical reaction, where there is no electron exchange in the reaction one can write as an equilibrium condition:

$$\Delta G_r^{0} = -RT\sum_{i=1}^{k}\ln(c_i)^{n_i} \tag{23}$$

The process of generating Pourbaix diagrams for an H_2S-H_2O-Fe system generally followed the steps shown in Figure 19.

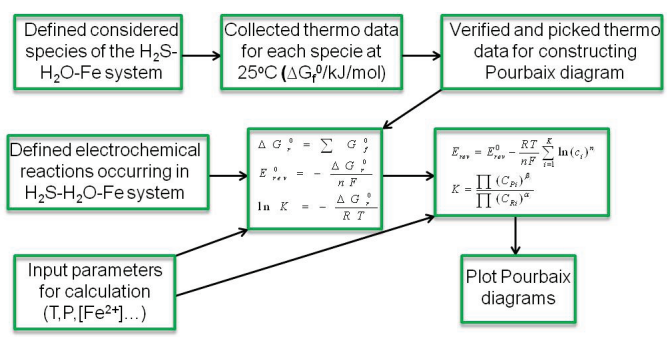

Figure 19. Process of generating Pourbaix diagrams.

The thermodynamic data for the considered species is listed in Table 5. The input parameters are shown in Table 6.

Table 5. Thermodynamic data of the considered species of H_2S-H_2O-Fe system.

Species	ΔG_f^0 (kJ/mol)	Source
H^+ (aq)	0	41
H_2S (g)	-33.329	42
H_2O (l)	-237.141	42
H_2 (aq)	17.74	41
O_2 (aq)	16.53	41
Fe (s)	0	42
Fe^{2+} (aq)	-91.5	41
Fe^{3+} (aq)	-17.24	41
Fe_2O_3 (s)	-743.523	42
Fe_3O_4 (s)	-1017.438	42
$Fe(OH)_2$ (s)	-491.969	42
$Fe(OH)_3$ (s)	-705.467	42
FeS (mackinawite) (s)	-100.07	calculated from Part II
Fe_3S_4 (greigite) (s)	-311.88	recalculated from [6]
FeS (pyrrhotite) (s)	-101.95	43
FeS_2 (pyrite) (s)	-160.06	43

Table 6. Input parameters.

Temperature / ^oC	25
P_{total} / bar	1
pH_2S / bar	0.0968 (10%)
$[Fe^{2+}]$ / mol/L	1.79×10^{-4} (10 ppm)
$[Fe^{3+}]$ / mol/L	1.0×10^{-6}
pH_2 / bar	1
pO_2 / bar	1

Pourbaix diagram for a H_2O-Fe System at 25^oC

To construct Pourbaix diagrams for an H_2S-H_2O-Fe system, the H_2O-Fe system was used as the simple starting point. All the equilibria for electrochemical and chemical reactions occurring in the H_2O-Fe system are listed in the second column in Table 7. The Nernst equation, Equation (18), is used for electrochemical reactions to calculate the reversible potential at equilibrium, and Equation (23) is used for chemical reactions to compute the equilibrium pH. The expressions for equilibrium potential and pH are shown in the last column in Table 7. Equation (19) is used to calculate the standard reversible potential, using the information derived in Table 5 and Table 6. The Pourbaix diagram for the H_2O-Fe system at 25^oC is created for arbitrary conditions similar to the author's test parameters and is shown in Figure 20.

Table 7. Equilibria of electrochemical reactions occurring in the H_2O-Fe system.

No.	Reaction	Equilibrium Potential or pH
H	$2H^+ + 2e^- \Leftrightarrow H_2$	$E_{rev(H^+/H_2)} = E^0_{rev(H^+/H_2)} - \frac{RT}{2F}\ln\frac{pH_2}{[H^+]^2}$
O	$O_2 + 4H^+ + 4e^- \Leftrightarrow 2H_2O$	$E_{rev(O_2/H_2O)} = E^0_{rev(O_2/H_2O)} - \frac{RT}{4F}\ln\frac{1}{pO_2\cdot[H^+]^4}$
1.	$Fe^{2+} + 2e^- \Leftrightarrow Fe$	$E_{rev(Fe^{2+}/Fe)} = E^0_{rev(Fe^{2+}/Fe)} - \frac{RT}{2F}\ln\frac{1}{[Fe^{2+}]}$
2.	$Fe^{3+} + e^- \Leftrightarrow Fe^{2+}$	$E_{rev(Fe^{3+}/Fe^{2+})} = E^0_{rev(Fe^{3+}/Fe^{2+})} - \frac{RT}{F}\ln\frac{[Fe^{2+}]}{[Fe^{3+}]}$
3.	$Fe^{2+} + 2H_2O \Leftrightarrow Fe(OH)_2 + 2H^+$	$pH_{(Fe^{2+}/Fe(OH)_2)} = -0.5\lg(K_{(Fe^{2+}/Fe(OH)_2)}[Fe^{2+}])$
4.	$Fe(OH)_2 + 2H^+ + 2e^- \Leftrightarrow Fe + 2H_2O$	$E_{rev(Fe(OH)_2/Fe)} = E^0_{rev(Fe^{3+}/Fe^{2+})} - \frac{RT}{2F}\ln\frac{1}{[H^+]^2}$
5.	$Fe_3O_4 + 2H_2O + 2H^+ + 2e^- \Leftrightarrow 3Fe(OH)_2$	$E_{rev(Fe_3O_4/Fe(OH)_2)} = E^0_{rev(Fe_3O_4/Fe(OH)_2)} - \frac{RT}{2F}\ln\frac{1}{[H^+]^2}$
6.	$6Fe_2O_3 + 4H^+ + 4e^- \Leftrightarrow 4Fe_3O_4 + 2H_2O$	$E_{rev(Fe_2O_3/Fe_3O_4)} = E^0_{rev(Fe_2O_3/Fe_3O_4)} - \frac{RT}{4F}\ln\frac{1}{[H^+]^4}$
7.	$Fe_3O_4 + 8H^+ + 2e^- \Leftrightarrow 3Fe^{2+} + 4H_2O$	$E_{rev(Fe_3O_4/Fe^{2+})} = E^0_{rev(Fe_3O_4/Fe^{2+})} - \frac{RT}{2F}\ln\frac{[Fe^{2+}]}{[H^+]^8}$
8.	$2Fe_2O_3 + 12H^+ + 4e^- \Leftrightarrow 4Fe^{2+} + 6H_2O$	$E_{rev(Fe_2O_3/Fe^{2+})} = E^0_{rev(Fe_2O_3/Fe^{2+})} - \frac{RT}{4F}\ln\frac{[Fe^{2+}]^4}{[H^+]^{12}}$
9.	$2Fe^{3+} + 3H_2O \Leftrightarrow Fe_2O_3 + 6H^+$	$pH_{(Fe^{3+}/Fe_2O_3)} = -\frac{1}{6}\lg(K_{(Fe^{3+}/Fe_2O_3)}[Fe^{3+}]^2)$

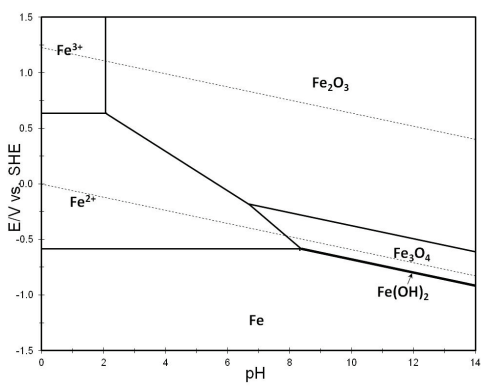

Figure 20. Pourbaix diagram for H_2O-Fe system at 25°C.

Pourbaix diagram with only Mackinawite in a H_2S-H_2O-Fe System at 25°C

Mackinawite is "added first" into the Pourbaix diagram for H_2O-Fe system, as it is the initial corrosion product in the presence of H_2S. The equilibria of reactions related to the formation of mackinawite (No.10-14) are listed in the second column in Table 8, the expressions for reversible potential and pH for each reaction are shown in the third column. When added into the H_2O-Fe system, and the graph, and after "cleaning up", the calculated equilibrium lines are shown in Figure 21 (a). Mackinawite and ferric oxide (Fe_2O_3) are observed in Figure 21 (a), while ferrous hydroxide ($Fe(OH)_2$) and magnetite (Fe_3O_4) have disappeared being less stable than mackinawite.

Pourbaix diagram with Mackinawite and Greigite in a H_2S-H_2O-Fe System at 25°C

The formation of greigite is considered next. The reactions (No.15-19) are taken into consideration, as Table 8 shows, and the correlations between the reversible potential and pH for these reactions are also shown in Table 8. Figure 21 (b) shows the Pourbaix diagram with mackinawite and greigite accounted for. Greigite is found in the higher potential range compared to mackinawite and significantly higher than would be typically seen in aqueous H_2S corrosion of mild steel.

Pourbaix diagram with Mackinawite, Greigite and Pyrrhotite in a H_2S-H_2O-Fe System at 25°C

The reactions related to the formation of pyrrhotite were incorporated next; reactions (No. 20-24) details shown in Table 8. The Pourbaix diagram with pyrrhotite added is shown in Figure 21 (c). Note that mackinawite is no longer present since it is replaced by the more thermodynamically stable product - pyrrhotite, which is the species to be expected in longer exposures under these conditions.

Pourbaix diagram with Mackinawite, Greigite, Pyrrhotite and Pyrite for H_2S-H_2O-Fe System at 25°C

The last of the dominant iron sulfides, pyrite, is added into the previous system. Reactions relating to the formation of pyrite (No. 25-31) are given in Table 8. Figure 21 (d) shows the Pourbaix diagram with all the four dominant iron sulfides considered. Only pyrrhotite and pyrite are present in Figure 21 (d), indicating these two phases are the final and thermodynamically stable iron sulfide corrosion products which are to be expected in long term exposures. Given the typical potential and pH range encountered during internal corrosion of mild steel in aqueous H_2S solutions, pyrrhotite should the main species expected in longer term exposures.

Table 8. Equilibria of electrochemical reactions occurring in the H_2S-H_2O-Fe system.

No.	Reaction	Equilibrium Potential or pH
10.	$FeS_m + 2H^+ + 2e^- \Leftrightarrow Fe + H_2S(g)$	$E_{rev(FeS_m/Fe)} = E^0_{rev(FeS_m/Fe)} - \frac{RT}{2F}\ln\frac{pH_2S}{[H^+]^2}$
11.	$FeS_m + 2H^+ \Leftrightarrow Fe^{2+} + H_2S(g)$	$pH_{(FeS_m/Fe^{2+})} = -0.5\lg(\frac{[Fe^{2+}]pH_2S}{K_{(FeS_m/Fe^{2+})}})$
12.	$Fe_2O_3 + 2H_2S(g) + 2H^+ + 2e^- \Leftrightarrow 2FeS_m + 3H_2O$	$E_{rev(Fe_2O_3/FeS_m)} = E^0_{rev(Fe_2O_3/FeS_m)} - \frac{RT}{2F}\ln\frac{1}{pH_2S^2\cdot[H^+]^2}$
13.	$Fe_3O_4 + 3H_2S(g) + 2H^+ + 2e^- \Leftrightarrow 3FeS_m + 4H_2O$	$E_{rev(Fe_3O_4/FeS_m)} = E^0_{rev(Fe_3O_4/FeS_m)} - \frac{RT}{2F}\ln\frac{1}{pH_2S^3\cdot[H^+]^2}$
14.	$Fe(OH)_2 + H_2S(g) \Leftrightarrow FeS_m + 2H_2O$	$K_{(Fe(OH)_2/FeS_m)} = \frac{1}{pH_2S}$
15.	$Fe_3S_4 + 8H^+ + 8e^- \Leftrightarrow 3Fe + 4H_2S(g)$	$E_{rev(Fe_3S_4/Fe)} = E^0_{rev(Fe_3S_4/Fe)} - \frac{RT}{8F}\ln\frac{pH_2S^4}{[H^+]^8}$
16.	$Fe_3S_4 + 8H^+ + 2e^- \Leftrightarrow 3Fe^{2+} + 4H_2S(g)$	$E_{rev(Fe_3S_4/Fe^{2+})} = E^0_{rev(Fe_3S_4/Fe^{2+})} - \frac{RT}{2F}\ln\frac{[Fe^{2+}]^3 pH_2S^4}{[H^+]^8}$
17.	$3Fe^{3+} + 4H_2S(g) + e^- \Leftrightarrow Fe_3S_4 + 8H^+$	$E_{rev(Fe_2O_3/Fe_3S_4)} = E^0_{rev(Fe_2O_3/Fe_3S_4)} - \frac{RT}{2F}\ln\frac{1}{[H^+]^2 pH_2S^8}$

18.	$3Fe_2O_3 + 8H_2S(g) + 2H^+ + 2e^- \Leftrightarrow 2Fe_3S_4 + 9H_2O$	$E_{rev(Fe_2O_3/Fe_3S_4)} = E^0_{rev(Fe_2O_3/Fe_3S_4)} - \frac{RT}{2F}\ln\frac{1}{[H^+]^2\, pH_2S^8}$
19.	$Fe_3S_4 + 2H^+ + 2e^- \Leftrightarrow 3FeS_m + H_2S(g)$	$E_{rev(Fe_3S_4/FeS_m)} = E^0_{rev(Fe_3S_4/FeS_m)} - \frac{RT}{2F}\ln\frac{pH_2S}{[H^+]^2}$
20.	$FeS_p + 2H^+ + 2e^- \Leftrightarrow Fe + H_2S(g)$	$E_{rev(FeS_{pyrrhotite}/Fe)} = E^0_{rev(FeS_{pyrrhotite}/Fe)} - \frac{RT}{2F}\ln\frac{pH_2S}{[H^+]^2}$
21.	$FeS_p + 2H^+ \Leftrightarrow Fe^{2+} + H_2S(g)$	$pH_{(FeS_{pyrrhotite}/Fe^{2+})} = \lg(\frac{pH_2S\cdot[Fe^{2+}]}{K_{(FeS_{pyrrhotite}/Fe^{2+})}})^{-\frac{1}{2}}$
22.	$Fe_2O_3 + 2H_2S(g) + 2H^+ + 2e^- \Leftrightarrow 2FeS_p + 3H_2O$	$E_{rev(Fe_2O_3/FeS_{pyrrhotite})} = E^0_{rev(Fe_2O_3/FeS_{pyrrhotite})} - \frac{RT}{2F}\ln\frac{1}{pH_2S^2\cdot[H^+]^2}$
23.	$Fe_3S_4 + 2H^+ + 2e^- \Leftrightarrow 3FeS_p + H_2S(g)$	$E_{rev(Fe_3S_4/FeS_{pyrrhotite})} = E^0_{rev(Fe_2O_3/FeS_{pyrrhotite})} - \frac{RT}{2F}\ln\frac{pH_2S}{[H^+]^2}$
24.	$FeS_{Pyrrhotite} \Leftrightarrow FeS_{Mackinawite}$	$K_{(FeS_p/FeS_m)} = 1$
25.	$FeS_2 + 4H^+ + 2e^- \Leftrightarrow Fe^{2+} + 2H_2S(g)$	$E_{rev(FeS_{2pyrite}/Fe^{2+})} = E^0_{rev(FeS_{2pyrite}/Fe^{2+})} - \frac{RT}{2F}\ln\frac{[Fe^{2+}]\cdot pH_2S^2}{[H^+]^4}$
26.	$FeS_2 + 4H^+ + 4e^- \Leftrightarrow Fe + 2H_2S(g)$	$E_{rev(FeS_{2pyrite}/Fe)} = E^0_{rev(FeS_{2pyrite}/Fe)} - \frac{RT}{4F}\ln\frac{pH_2S^2}{[H^+]^4}$
27.	$2FeS_2 + 3H_2O + 2H^+ + 2e^- \Leftrightarrow Fe_2O_3 + 4H_2S(g)$	$E_{rev(FeS_{2pyrite}/Fe_2O_3)} = E^0_{rev(FeS_{2pyrite}/Fe_2O_3)} - \frac{RT}{2F}\ln\frac{pH_2S^4}{[H^+]^2}$
28.	$FeS_2 + 2H^+ + 2e^- \Leftrightarrow FeS_{Mackinawite} + H_2S(g)$	$E_{rev(FeS_{2pyrite}/FeS_m)} = E^0_{rev(FeS_{2pyrite}/FeS_m)} - \frac{RT}{2F}\ln\frac{pH_2S}{[H^+]^2}$
29.	$FeS_2 + 2H^+ + 2e^- \Leftrightarrow FeS_{Pyrrhotite} + H_2S(g)$	$E_{rev(FeS_{2pyrite}/FeS_{pyrrhotite})} = E^0_{rev(FeS_{2pyrite}/FeS_{pyrrhotite})} - \frac{RT}{2F}\ln\frac{pH_2S}{[H^+]^2}$
30.	$FeS_2 + 4H^+ + e^- \Leftrightarrow Fe^{3+} + 2H_2S(g)$	$E_{rev(FeS_{2pyrite}/Fe^{3+})} = E^0_{rev(FeS_{2pyrite}/Fe^{3+})} - \frac{RT}{F}\ln\frac{[Fe^{3+}]\cdot pH_2S^2}{[H^+]^4}$
31.	$3FeS_2 + 4H^+ + 4e^- \Leftrightarrow Fe_3S_4 + 2H_2S(g)$	$E_{rev(FeS_{2pyrite}/FeS_{greigite})} = E^0_{rev(FeS_{2pyrite}/FeS_{greigite})} - \frac{RT}{4F}\ln\frac{pH_2S^2}{[H^+]^4}$

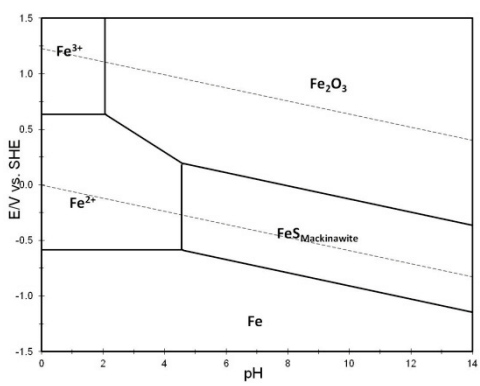

(a) Mackinawite

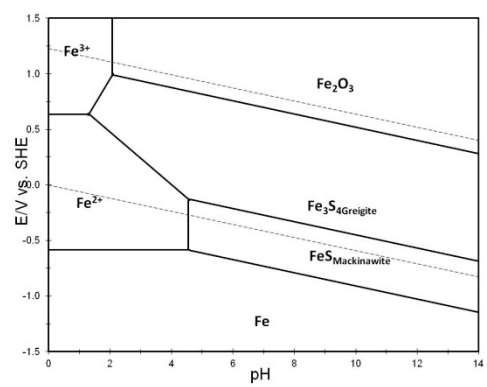

(b) Mackinawite/Greigite

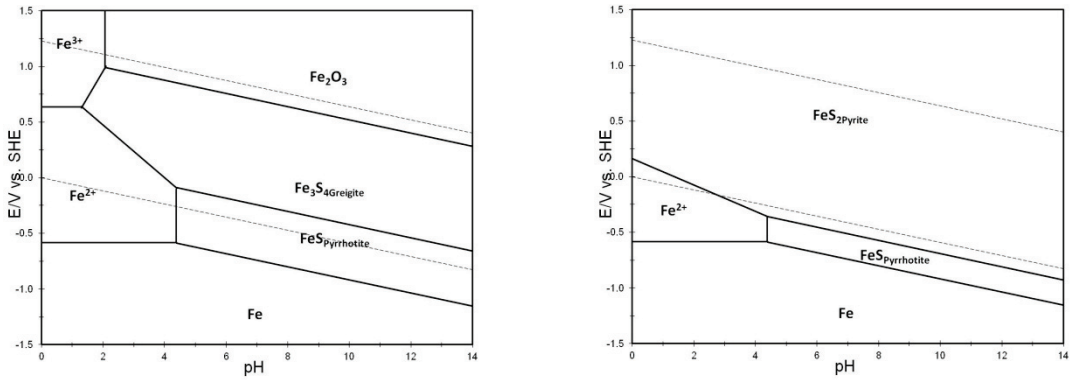

(c) Mackinawite/Greigite/Pyrrhotite (d) Mackinawite/Greigite/Pyrrhotite/Pyrite

Figure 21. Pourbaix diagram for H_2S-H_2O-Fe system.

Summary

The key polymorphous iron sulfides relevant for corrosion of mild steel in oil and gas systems have been identified to be: mackinawite (FeS), greigite (Fe_3S_4), pyrrhotite ($Fe_{1-x}S$, x=0 to 0.17) and pyrite (FeS_2).The Pourbaix diagrams of H_2S-H_2O-Fe system at 25^oC were constructed indicating that under typical conditions seen during internal corrosion of mild steel in aqueous H_2S containing solutions (potential and pH range) mackinawite should be expected in shorter exposures while pyrrhotite should be the key corrosion product seen in longer exposures. Due to fast kinetics, mackinawite should be the most common species seen in short exposures. Greigite and pyrite are more likely to form at higher pH and higher potentials, more typical for oxygenated solutions.

ACKNOWLEDGEMENTS

The authors would like to express sincere appreciation to the following industrial sponsors for their financial support and direction: BG Group, BP, Champion Technologies, Chevron, Clariant Oil Services, ConocoPhillips, Encana, ENI S.P.A., ExxonMobil, WGIM, NALCO Energy Services, Occidental Oil Company, Petrobras, PETRONAS, PTT, Saudi Aramco, INPEX Corporation, Total, TransCanada. The authors also appreciate the help offered at the Center for Electrochemical Engineering Research, Department of Chemical and Biomolecular Engineering at Ohio University, enabling the use of the XRD equipment.

REFERENCES

1. W. Sun, S. Nesic, D. Young and R. Woolam, “Equilibrium expressions related to the solubility of the sour corrosion product mackinawite,” *Ind. Eng. Chem. Res.*, vol. 47, pp. 1738-1742, 2008.
2. O. M. Suleimenov and R. E. Krupp, “Solubility of hydrogen sulfide in pure water and in NaCl solutions, from 20 to 320^oC and at saturation pressures,” *Geochim. Cosmochim. Ac.*, vol. 58, no.11, pp. 2433-2444, 1994.
3. O. M. Suleimenov and T. M. Seward, “A spectrophotometric study of hydrogen sulfide ionization in aqueous solutions to 350^oC,” *Geochim. Cosmochim. Ac.*, vol. 61, no. 24, pp. 5187-5198, 1997.

4. Y. K. Kharaka, E. H. Perkins, W. D. Counter, J. D. Debral, and C. H. Bamford, *Solmineq 88:A Computer Program for Geochemical Modeling of Water Rock Interactions*, Menlo park, CA: Alberta Research Council, 1989.
5. L. G. Benning, R. T. Wilkin, and H. L. Barnes, "Reaction pathways in the FeS below 100°C," *Chem. Geol.*, vol. 167, pp. 25-51, 2000.
6. R. A. Berner, "Thermodynamic stability of sedimentary iron sulfides," *A. J. of Science*, vol. 265, pp. 773-785, Nov. 1967.
7. J. W. Morse, F. J. Millero, J. C. Cornwell, and D. Rickard, "The chemistry of hydrogen sulfide systems in natural waters", *Earth Sci. Reviews*, vol. 24, pp. 1-42, 1987.
8. S. Theberge and G. W. Luther, "Determination of the electrochemical properties of a soluble aqueous FeS species present in sulfidic solutions," *Aquat. Geochem.*, vol. 3, pp. 191-211, 1997.
9. D. Rickard, "The solubility of FeS," *Geochim. Cosmochim. Ac.*, vol. 70, pp. 5779-5789, 2006.
10. Craig, and D. Bruce, "The nature of iron sulfides formed on steel in an H_2S-O_2 environment," *Corrosion*, vol. 35, pp. 136-138, 1979.
11. J. A. Bourdoiseau, M. Jeannin, R. Sabot, C. Remazeilles and Ph. Refait, "Characterisation of mackinawite by Raman spectroscopy: Effects of crystallization, drying and oxidation," *Corros. Sci.*, vol. 50, pp. 3247-3255, 2008.
12. W. Davison, "The solubility of iron sulfides in synthetic and natural waters at ambient temperature," *Aquat. Sci.*, vol. 53, pp. 309-329, 1991.
13. D. Rickard and G. W. Luther, "Chemistry of iron sulfides," *Chem. Rev.*, vol. 107, pp. 514-562, 2007.
14. P. Taylor, "The stereochemistry of iron sulfides-a structural rationale for the crystallization of some metastable phases from aqueous solution," *Am. Mineral.*, vol. 65, pp. 1026-1030, 1980.
15. J. S. Smith and J. D. A. Miller, "Nature of sulfides and their corrosive effect on ferrous metals: a review," *Brit. Corros. J.*, vol. 10, pp. 136-143, 1975.
16. S. N. Smith, B. Brown and W. Sun, "Corrosion at higher H_2S concentrations and moderate temperatures," presented at Corrosion/2011, NACE International, Houston, TX, 2011, Paper 11081.
17. W. Sun, "Kinetics of iron carbonate and iron sulfide scale formation in carbon dioxide/hydrogen sulfide corrosion," Ph.D. dissertation, Dept. Chem. Eng, Ohio Univ., Athens, OH, 2006.
18. K. Lee, "A mechanistic modeling of CO_2 corrosion of mild steel in the presence of H_2S," Ph.D. dissertation, Dept. Chem. Eng, Ohio Univ., Athens, OH, 2004.
19. M. Singer, A. Camacho, B. Brown, and S. Nesic, "Sour top of the line corrosion in the presence of acetic acid," presented at Corrosion/2010, NACE International, Houston, TX, 2010, Paper 10100.
20. M. Singer, S. Nesic, and J. N. Al-Khamis, "Corrosion assessment in Karan gas field development," presented at Corrosion/2012, NACE International, Houston, TX, 2012, Paper 0001411.
21. S. N. Smith and M. Joosten, "Corrosion of carbon steel by H_2S in CO_2 containing oilfield environments," presented at Corrosion/2006, NACE International, Houston, TX, 2006, Paper 06115.
22. S. N. Smith, "A proposed mechanism for corrosion in slightly sour oil and gas production," presented at 12th International Corrosion Congr., Houston, TX, Sept. 19-24, 1993, Paper 385.
23. W. A. Kornicker, "Interactions of divalent cations with pyrite and mackinawite in seawater and NaCl solutions". Ph. D. Dissertation, Texas A&M Univ., TX, 1988.

24. M. Wolthers, S. J. Van der Gaast, and D. Rickard, “The structure of disordered mackinawite”, *Am. Mineral.*, vol. 88, pp. 2007–2015, 2003.
25. D. Rickard, A. Griffith, A. Oldroyd, I. B. Butler, E. Lopez-Capel, D. A. C. Manning, and D. C. Apperley, “The composition of nanoparticulate mackinawite, tetragonal iron(II) monosulfide,” *Chem. Geol.*, vol. 235, pp. 286–298, 2006.
26. J. W. Morse, and D. Rickard, “Chemical Dynamics of sedimentary acid volatile sulfide,” *Environ. Sci. Technol.*, pp. 131-136, 2004.
27. R. E. Sweeney, and I. R. Kaplan, “Pyrite Framboid Formation; Laboratory Synthesis and Marine Sediments,” *Econ. Geol*., vol. 68, pp. 618-634, 1973.
28. J. C. Ward, “The structure and properties of some iron sulfides,” *ReV. Pure Appl. Chem.*, vol. 20, pp. 175-206, 1970.
29. A. R. Lennie, and D. J. Vaughan, “Spectroscopic studies of iron sulfide formation and phase relations at low temperatures”. Presented at Mineral Spectroscopy: A Tribute to Roger G. Burns; Dyar, M. D., McCammon, C., Schaefer, M. W., Eds.; The Geochemical Society: Houston, TX, 1996, vol. 5, pp. 117-131.
30. D. Rickard, A. Griffith, A. Oldroyd, I.B. Butler, E. Lopez-Capel, D. A. C. Manning, and D. C. Apperley, “The composition of nanoparticulate mackinawite, tetragonal iron(II) monosulfide,” *Chem. Geol.*, vol. 235, pp. 286–298, 2006.
31. D. Medicis, and Rinaldo, "Cubic FeS, a Metastable Iron Sulfide," *Science*, vol. 170, pp. 1191-1192, 1970.
32. B. J. Murowchick, and H. L. Barnes, "Formation of Cubic FeS," *Am. Mineral.*, vol. 71, pp. 1243-1246, 1986.
33. R.G. Arnold, "Pyrrhotite phase relations below 304°C at <1 atm total pressure," *Econ. Geol.*, vol. 64, pp. 405-419, 1969.
34. M. Schoonen, and H. L. Barnes, “Reactions forming pyrite and marcasite from solution: II. Via FeS precursors below 100°C,” *Geochim. Cosmochim. Ac.*, vol. 55, pp. 1505-1514, 1991.
35. M. Pourbaix, “Atlas of electrochemical equilibria in aqueous solutions,” presented at NACE, Houston, TX, 1974.
36. M. Pourbaix, *Lectures on Elctrochemical Corrosion*, Translated from the French by J.A.S. Green, Plenum Press, London and New York, 1973.
37. J. Bouet, J. P. Brenet, “Contribution a l’etude du diagramme tension/pH du fer en milieu sulfures,” *Corros. Sci.*, vol. 3, pp. 51-63, 1963.
38. M. Ueda, “Potential-pH diagram at elevated temperatures for metal-CO2/H2S-water systems and the application for corrosion of pure iron,” *Corros. Eng*., vol. 44(3), pp.159-174, 1995.
39. A. Anderko, P. J. Shuler, “A computational approach to predicting the formation of iron sulfide species using stability diagrams,” *Computers & Geosciences*, vol. 23 (6), pp.647-658, 1997
40. A. Anderko, S. J. Sanders, R. D. Young, “Real-solution stability diagrams: a thermodynamic tool for modeling corrosion in wide temperature and concentration ranges,” *Corros. Sci.*, vol. 53(1), pp. 43-53, 1997.
41. E. H. Oelkers, H. C. Helgeson, et. al., "Summary of the apparent standard partial molal gibbs free energies of formation of aqueous species, minerals, and gases at pressures 1 to 5000 bars and temperatures 25 to 1000°C," *J. Phys. Chem. Ref. Data*, vol. 24(4), pp. 1401-1560, 1995.
42. M.W. Chase, J. R. Downey, *JANAF thermochemical tables*, 4th ed., Natl. Stand. Ref. Data Ser., 1998.
43. M. W. Chase, C. A. Davies, J. R. Downey, D. J. Fruip, R. A. Madonald, and A. N. Syverud, JANAF thermochemical tables, 3rd ed., *J. Phys. Chem. Ref. Data*, vol. 14(1), pp. 1-1856, 1985.